

1 **Seismic Anisotropy from the Variscan Core of Iberia to the Western African Craton:**  
2 **New Constrains on Upper Mantle Flow at Regional Scales.**

3

4 J. Díaz and J. Gallart

5 Institute of Earth Sciences J. Almera, ICTJA-CSIC

6 c/ Sole Sabaris s/n, 08028 Barcelona, Spain.

7 Tel.: +34 934095410 e-mail: [jdiaz@ictja.csic.es](mailto:jdiaz@ictja.csic.es)

8

9

10 **Abstract**

11

12 The regional mantle flow beneath the westernmost Mediterranean basin and its transition to  
13 the Atlantic domain is addressed by inspecting the anisotropic properties of the mantle. More  
14 than 100 new sites, from the Variscan core of Iberia to the northern rim of the Western  
15 African Craton, are now investigated using the data provided by different temporary and  
16 permanent broad-band seismic arrays. Our main objective is to provide a larger regional  
17 framework to the results recently presented along the Gibraltar Arc in order to check the  
18 validity of the different geodynamic interpretations proposed so far.

19

20 The significant variations in the retrieved anisotropic parameters suggest that different  
21 processes must be invoked to explain the origin of the observed anisotropy. Beneath the  
22 Variscan units of the Central Iberian Massif the new results show a moderate amount of  
23 anisotropy with fast polarization directions (FPD) oriented close to E-W. Those results can  
24 only be explained in terms of global mantle flow if models accounting for contributions from  
25 surface plate motion, net lithosphere rotation and density variations are taken into  
26 consideration. One of the major results presented is the significant number of good quality  
27 data without evidence of anisotropy (“nulls”) observed beneath permanent stations in southern  
28 Portugal. Those “nulls” can be explained by the presence of a predominantly vertical mantle  
29 flow associated to large variations in the lithospheric thickness. Beneath the Gibraltar Arc the  
30 FPD show a spectacular rotation, evidenced by the results presented by Diaz et al. (2010) and  
31 Miller et al. (2013). Those results are reviewed here taking also into consideration the  
32 geodynamic modeling presented recently by Alpert et al. (2013) and other geophysical and  
33 geodetic results. Further South, the analysis of new broad-band stations installed in the

34 Moroccan Meseta and the High Atlas show a small degree on anisotropy and a large number  
35 of “null” events, pointing again to the presence of vertical flow in the mantle.

36

37 The results favor an asthenospheric origin related to present-day mantle flow for the  
38 anisotropy observed from the Variscan core of Iberia to the northern rim of the West African  
39 Craton. This flow is deflected around the high velocity slab beneath the Gibraltar Arc and  
40 seems affected locally by vertical flow associated to edge-driven convective cells. The  
41 presence of significant backazimuthal variations in the anisotropic parameters retrieved from  
42 single events suggests that a second order contribution from an anisotropic layer within the  
43 lithosphere may also exist.

44

79

80 The origin of the upper mantle anisotropy has been classically related to the strain-induced  
81 lattice preferred orientation (LPO) of the mantle minerals, in particular of olivine (e.g.,  
82 Nicolas and Christensen, 1987). Anisotropy thus provides one of the best tools to investigate  
83 deformation in the upper mantle, in a way extending structural geology. In tectonically active  
84 areas, fast polarization directions (FPD) are expected to mark the direction of flow. In zones  
85 without present-day large-scale tectonic activity, LPO results from strain from the last  
86 significant tectonic episode preserved in the subcrustal lithosphere or from dynamic flow in  
87 the asthenosphere. Therefore, even if it involves some ambiguity, the knowledge of the  
88 anisotropic properties can provide new clues on the geodynamic processes beneath the  
89 investigated area.

90

91

## 92 **2 Data acquisition and processing**

93

94 Until the last decade, very scarce data regarding the presence of anisotropy in the southern  
95 part of the Iberian Peninsula were available (Díaz et al., 1996, Díaz et al., 1998, Calvert et al,  
96 2000, Serrano et al., 2005). The installation of new permanent and semi-permanent broad-  
97 band stations in the Betics area allowed a first regional reconnaissance of its anisotropic  
98 properties (Buontempo et al, 2008), documenting geographical variations in the anisotropic  
99 parameters, even if only a few sites in N Morocco could be studied. Later on, with the  
100 installation of the much denser TopoIberia network, the knowledge of the anisotropic features  
101 beneath the Gibraltar Arc was significantly improved (Díaz et al. 2010). The contribution of  
102 the PICASSO network has recently increased the data density along a North-South transect  
103 and has allowed the first numerical flow modeling beneath the area (Miller et al., 2013, Alpert  
104 et al., 2013).

105

106 In this contribution, we expand the previously published data with new measurements coming  
107 from seismic stations installed over a wider geographic region. From North to South, we have  
108 used the data provided by the second TopoIberia-Iberarray deployment, covering the central  
109 part of the Iberian Peninsula, additional TopoIberia stations installed over the Moroccan  
110 Meseta and the High Atlas, and the temporary deployment carried out by the Univ. of  
111 Munster and the Univ. of Bristol in the framework of the Comitac project that covers the  
112 western High Atlas and the Anti-Atlas domain. We also had access to the data from two short-

## 45 **1 Introduction**

46

47 The Western Mediterranean area has a complex geodynamic evolution the main points of  
48 which are still under debate and that result in a zone with clear extensional features in the  
49 framework of a compressional regime related to the present-day collision between Nubia and  
50 Eurasia. Moving further west, the Atlantic margin, and in particular the Gulf of Cadiz, show  
51 also a great degree of complexity; with a poorly defined plate boundary, the presence of  
52 historic large magnitude seismicity and a sustained amount of small to moderate seismicity at  
53 subcrustal depths. An appropriate way to try to discern between the different geodynamic  
54 hypotheses proposed is the acquisition and interpretation of larger amounts of geophysical  
55 data, even if this often leads to more complex images than those proposed by theoretical  
56 modeling. During the last years, large scale projects such as TopoIberia (Díaz et al., 2009) and  
57 PICASSO have been designed with this objective. Up to now, the main focus has been  
58 centered in the Gibraltar Arc System (Platt and Vissers, 1989) which has been investigated by  
59 magnetotelluric profiles (Anahnah et al., 2011; Ruiz-Constán et al., 2012), local and  
60 teleseismic tomography (Villaseñor et al., 2011, El Moudnib et al, 2012; Bezada et al, 2013),  
61 surface wave tomography (Palomeras et al., 2012), crustal structure derived from receiver  
62 function analysis (Mancilla et al., 2012; Thurner et al., 2012) and wide-angle  
63 reflection/refraction profiles (Gallart et al., 2012) or mantle anisotropy (Díaz et al. 2010,  
64 Miller et al., 2013, Alpert et al., 2013).

65

66 The main objective in this contribution is to present and analyze the new anisotropic  
67 parameters obtained from shear-wave splitting data beneath a large area including, North to  
68 South, from the Variscan Central Iberian Massif of Iberia to the northern rim of the West  
69 African Craton and, East to West, from the Algerian basin to the Atlantic domain. Those new  
70 results provide a wider framework to the anisotropic results presented recently in the Gibraltar  
71 arc by Diaz et al 2010 and Miller et al. (2013) and allow reviewing the geodynamic modeling  
72 presented by Alpert et al. (2013) as it allows a better understanding of the interactions of the  
73 Gibraltar Arc with the surrounding, more stable regions. To achieve this purpose, we have  
74 gathered data from different permanent and temporary broad-band networks installed over the  
75 investigated region, including some over the marine areas covered by short term ocean bottom  
76 seismometer (OBS) deployments. The final data set allows the calculation of anisotropic  
77 parameters over a large number of stations and facilitates the geodynamic interpretation of the  
78 results.

113 term broad-band OBS deployments in the Alboran Sea and Gulf of Cadiz installed by Geomar  
114 as part of the Topomed project. Finally, we have gathered data from the permanent networks  
115 in Spain, Portugal and Morocco (Figure 1). This has resulted in a dataset comprising 106  
116 stations to be added to the 92 sites investigated previously by Díaz et al., (2010) and the 81  
117 sites, mostly along a dense profile oriented N-S, presented by Miller et al (2013).

118

119 The different deployments are not completely coincident in time. Time intervals of about 12  
120 to 18 months have been inspected for each station within a time interval between summer  
121 2009 and the end of 2011 (Supplemental Table 1). The OBS were deployed firstly in the  
122 Alboran Sea for 4 months and later in the Gulf of Cadiz during 6 months. This rather short  
123 time interval, together with the intrinsic problems in recording seismic signals at long periods  
124 undersea (noise, coupling, sensor orientation), made it possible to retain only some  
125 anisotropic measurements at each instrument. All the events with magnitude greater than 6.0-  
126 6.2 and epicentral distances ranging between  $90^\circ$  and  $130^\circ$  have been inspected and up to 130  
127 events have finally provided useful anisotropic measurements. Due to the dominant period of  
128 the inspected SKS waves, it is difficult to get accurate measurements of very small delay  
129 times. As a general rule, only the events with delay times greater than 0.4s are classified as  
130 anisotropic.

131

132 To inspect this large amount of data we have benefited from the SplitLab software (Wüstefeld  
133 et al., 2006), that provides a useful tool to measure the splitting parameters and manage the  
134 resulting database. Most of the results have been obtained using the method based on the  
135 search for a maximum correlation between the two quasi-shear waves (Figure 2), as it is less  
136 sensitive to possible misorientations of the seismometer horizontal components than the  
137 methods based on the minimization of the transverse component energy (Tian et al., 2011). In  
138 a few particular cases we preferred to retain the result from this last method as it provided a  
139 more realistic adjustment. We have used the usual quality criteria in anisotropic studies, based  
140 firstly on a good signal-to-noise ratio allowing clear phase identifications and, secondly, in the  
141 linearization of the particle motion and the retrieval of the backazimuthal direction once the  
142 anisotropic effect has been corrected. According to those criteria, events were classified into  
143 three categories (good, fair, poor) and only those in the firsts two classes were further used.  
144 Measurements providing small delay times relative to the dominant period of the SKS waves,  
145 (around 6-8 s) are interpreted as “nulls”, that is, as not showing evidence of anisotropy.  
146 However, in the presence of noise some of those “nulls” can simply correspond to unstable

147 measurements. To avoid this misinterpretation we have only retained as “nulls” the good  
148 measurements providing delay times smaller than 0.25s and we have discarded the  
149 measurements with delay times between 0.25 and 0.4 s. This resulted in a total of 981 non-  
150 null and 404 null measurements. For most of the stations we have retained 10 to 20  
151 observations, with a mean value of 16.2 valid measurements per station. Supplemental Table  
152 1 shows the mean FPD and delay time for each analyzed station as well as the corresponding  
153 standard deviation. The individual results are presented in the Supplemental Table 2 and  
154 displayed in Figure 3. We have checked the stability of the results by retaining only those  
155 cases for which the difference between the results from the maximum correlation and  
156 transverse energy minimization methods does not exceed 20° for FPD and 0.3s for  $\delta t$ . Even if  
157 the amount of individual measurements decreases a 40% under those restrictive conditions,  
158 the general anisotropic pattern remains nearly unchanged (see Supplemental Table 2).

159

160

### 161 **3 Results**

162

163 The investigated area encompasses very different tectonic units, from the Variscan units of  
164 Central Iberia to the West African Craton (WAC). We will summarize our results, presented  
165 in Figure 3, for each different unit.

166

167 To the North, the central and western part of Iberia corresponds to the Variscan Central  
168 Iberian Massif (CIM), which has remained tectonically stable for the last 300 Ma, since the  
169 end of the Hercynian orogeny (Gibbons and Moreno, 2002). The anisotropic parameters  
170 retrieved over this area are quite uniform, with FPDs oriented close to E-W and a moderate  
171 degree of anisotropy, with  $\delta t$  values around 1.0 s. The eastern part of central Iberia is  
172 dominated by Meso-Tertiary zones reworked by the Alpine orogeny. The anisotropic  
173 parameters remain similar to those reported for the CIM, even if the amount of anisotropy  
174 seems to increase slightly. The easternmost area is dominated by the extension associated to  
175 the opening of the Valencia Trough in Neogene time, as a result of the clockwise rotation of  
176 the Balearic block (Dewey et al., 1989). The FPD obtained at the Balearic Islands also show a  
177 dominant E-W trend beneath the western islands, but with a significant shift to ESE-WNW  
178 beneath the easternmost island of Menorca.

179

180 Further South, the western part of the investigated area still corresponds to the Variscan  
181 Massif, in this case formed by the South-Portuguese and the Ossa-Morena units, both accreted  
182 to the Central Iberian Massif in Carboniferous times and geologically stable for the last 300  
183 Ma (Gibbons and Moreno, 2002). The most relevant observation derived from the analysis of  
184 permanent stations in southern Portugal is the presence of a large number of events with clear  
185 SKS arrivals without any evidence of anisotropy, commonly identified as “nulls”. For the rest  
186 of the cases, the FPD inferred from individual events show large variations, even if a  
187 dominant NE-SW direction can be identified. The delay times are small, in the 0.5-0.8s range.  
188 As will be discussed later on, those facts suggest a geodynamic complexity which is not  
189 directly related to the surface geology.

190

191 The eastern part of South Iberia and the northern part of Morocco are formed by the so-called  
192 Gibraltar Arc System (Platt and Vissers, 1989). This system has classically been divided in  
193 three domains; the internal zone formed mainly by metamorphic units, the external zone,  
194 formed mainly by piled-up slices of the sedimentary cover of the paleo margin and the  
195 Alboran basin, which corresponds to the extensional back-arc domain. The results over this  
196 zone have already been presented and discussed in Díaz et al. (2010) and have been  
197 confirmed recently by Miller et al. (2013) using a denser deployment focused along a N-S  
198 profile. The main feature observed is the spectacular rotation of the FPD along the Gibraltar  
199 arc following the curvature of the Rif-Betic chain, from roughly N65°E beneath the Betics to  
200 close to N65°W beneath the Rif chain. Additionally, a clear change is observed between the  
201 internal Rif and the external and foreland units. New data from the OBSs deployed in the  
202 Alboran Sea, even if limited in number and quality, show a small degree of anisotropy, with  
203 FPD oriented mostly E-W and quite consistent with previous results in the permanent station  
204 located at the Alboran Island.

205

206 The Gulf of Cadiz lies at the eastern termination of the Azores-Gibraltar fracture zone and has  
207 also a complex structure, including a change from extensional tectonics in the West to mostly  
208 compressional in the East, the transition from oceanic to continental crust (Sallarès et al.,  
209 2012) and the presence of significant seismicity around 70 km depth (Buforn et al., 2004).  
210 OBSs located in the western part of the gulf show a North-South component in the inferred  
211 FPDs, while in the central zone the FPDs are closer to E-W. However, few measurements are  
212 available and thus those results must be taken with caution.

213

214 Northern Morocco can be divided into three main tectonic domains; the Rif Chain, the  
215 Meseta-Atlasic domain and the Anti-Atlas domain, corresponding to the northern limit of the  
216 WAC (Michard et al., 2008). The Meseta-Atlasic domain is formed in turn by the Moroccan  
217 Meseta, the High Atlas and the Middle Atlas. Díaz et al., (2010) show a clear change in FPD  
218 between the Rif and the northern part of the Middle Atlas. Miller et al., (2013), confirmed this  
219 point and extended the available anisotropic measurements further South along a profile  
220 crossing the Atlas, getting small  $\delta t$  (0.6 – 0.9 s) and FPD oriented ENE-WSW. The new data  
221 presented here show similar results for sites in the central part of the Moroccan Meseta as  
222 well as in the central and western sections of the High Atlas. Further South, the northern rim  
223 of the WAC, the Anti-Atlas domain, is explored using the data provided by the Comitac  
224 network, also used by Miller et al. (2013). Most of the stations show a small degree of  
225 anisotropy (0.5 - 0.8 s) and FPD not far from E-W. It is important to note that, as already  
226 described for SW Portugal, there is a large number of high quality events without evidence  
227 for anisotropy ("nulls") beneath the western part of the High Atlas and Anti-Atlas units.

228

229

#### 230 **4 Geodynamic interpretation**

231

232 In order to progress from the observation of anisotropy on seismic data to their interpretation  
233 in geodynamic terms, three steps are needed. Firstly, we need to identify the effect of  
234 anisotropy in the data. In this contribution we used one of the most robust effects of seismic  
235 propagation through an anisotropic medium, the birefringence or splitting of the SKS shear-  
236 waves. This phenomenon has been widely investigated and the techniques to identify it have  
237 now become routinely used.

238 As a second step, we need to explain the process that originates the observed anisotropy. Even  
239 if Fichtner et al. (2013) have suggested that the observed seismic anisotropy can often be  
240 explained by purely isotropic layering, it remains widely accepted that anisotropy in the  
241 mantle is related to the lattice preferred orientation (LPO) of the minerals, in particular  
242 olivine, which is the major constituent of the upper mantle (Nicolas and Christensen, 1987).  
243 LPO patterns in peridotites measured in laboratory show that in most of the cases, the fast  
244 propagation axes align with the direction of maximum shear, allowing relating anisotropy and  
245 strain. However, factors such as temperature, melt fraction or presence of water result in  
246 changes in the olivine fabric and its relationship with deformation (Long and Becker, 2010).  
247 Other mechanisms, such as the presence of melt pockets or the preferred orientation of cracks



248 in the upper crust can also play a significant role in the origin of the anisotropy (Savage,  
249 1999).

250 Finally, the last step is to discuss the tectonic process responsible for the deformation. One  
251 good candidate, in particular for tectonically active areas, is the existence of a present-day  
252 asthenospheric flow that dynamically produces the observed LPO. In a classical interpretation  
253 (Vinnik et al., 1989), the passive motion of the lithosphere over the asthenospheric mantle  
254 will result in FPD oriented parallel to the absolute plate motion. At a global scale, the  
255 anisotropic parameters inferred from SKS and surface waves have been used to derive new  
256 mantle flow models taking into consideration not only the surface plate motions but also the  
257 effect of lateral heterogeneity in viscosity, which induce net lithosphere rotation, and the  
258 presence of density-driven flow (Becker, 2008, Kreemer, 2009, Conrad and Behn, 2010).  
259 Alternatively, the origin of the observed anisotropy can be related to the last tectonic event  
260 affecting the region, whose strain would have been preserved, “frozen-in”, in the subcrustal  
261 lithosphere. This mechanism has often been invoked to explain anisotropic observations in  
262 passive areas. Under this hypothesis, the FPD are expected to be parallel to major structures,  
263 such as plate boundaries or mountains belts. It is important to note that the major limitation of  
264 the shear-wave splitting measurements is its lack of vertical resolution, as we can only  
265 measure the integrated effect of anisotropy along the raypath. We know that the contribution  
266 of the crust is limited to few tens of second and it is widely accepted that most of the  
267 anisotropy comes from the upper mantle, even if it remains unclear whether anisotropy is  
268 confined to the upper 200 km or continues through the transition zone (Savage, 1999).  
269 Therefore, SKS measurements cannot identify if the main source of anisotropy lies in the  
270 lithosphere or the asthenosphere and hence discriminate between the above hypotheses.  
271 However, with the availability of large amounts of anisotropic observations worldwide, it  
272 seems clear that, in particular for continental areas, the anisotropy is a complex phenomenon  
273 that probably involves contributions both at lithospheric and asthenospheric levels.

274

275 Beneath central Iberia, the retrieved FPD are rather uniform, oriented close to E-W and with  
276  $\delta t$  around 1.0 s. This orientation is difficult to interpret in terms of “frozen-in” anisotropy  
277 related to a Variscan deformation preserved in the lithosphere, as the retrieved FPD clearly  
278 differ from the surface expression of the Variscan orogeny, with tectonic lineaments oriented  
279 close to NW-SE in the southern part of Iberia and shifting smoothly to N-S in NW Iberia  
280 following the arcuate Variscan belt (Matte, 1991). Global plate tectonic models assuming no  
281 net rotation, determined solely from the relative motions between plates, give an absolute

282 plate motion (APM) vector oriented close to NE (N50°E) beneath Iberia. Models obtained  
283 within a hot spot based reference frame, and thus assuming net rotation of the tectonic plates,  
284 result in a nearly opposite direction, close to WSW (N238°E). In both cases the speed is low,  
285 around 20 mm/year ([http://www.unavco.org/community\\_science/science-  
286 support/crustal\\_motion/dxdt/model.html](http://www.unavco.org/community_science/science-support/crustal_motion/dxdt/model.html)). Neither of those directions is parallel to the FPD  
287 observed beneath Central Iberia, as would be expected if the anisotropy was due to present-  
288 day mantle flow. However, a viscous mantle flow model presented by Conrad and Behn  
289 (2010) taking into consideration the contributions to global flow of plate tectonics, mantle  
290 density heterogeneity and net lithosphere rotation results in a flow field at upper mantle  
291 depths (200-400 km) oriented E-W beneath central Iberia, which is compatible with our  
292 splitting measurements (Figure 4a). This model is also consistent with the previous splitting  
293 measurements in northern Iberia (Supplementary Figure 1), showing N-E oriented FPD (Díaz  
294 et al., 2006) as well as the results beneath the Pyrenees, where the FPD is oriented ESE-  
295 WNW (Barruol et al., 1998).

296

297 Results beneath the Balearic Islands also show E-W FPD beneath the western islands, but the  
298 results shift to ESE-WNW beneath the easternmost island of Menorca. This FPD change  
299 could be related to the differential rotation affecting the Balearic Islands and the Corsica-  
300 Sardinia block in Late Oligocene-Early Miocene times. Barruol et al. (2004) interpreted the  
301 FPD variations observed in SE France and Corsica as an evidence of mantle flow preserved in  
302 the deep lithosphere since the end of the Cenozoic extensive episode. However, more  
303 information on the anisotropic parameters beneath the eastern termination of the Pyrenees and  
304 Sardinia is needed to properly discuss the origin of anisotropy in this region.

305

306 Díaz et al. (2010) suggested that the spectacular rotation of the FPD along the Gibraltar Arc  
307 may be the outcome of two processes; an active mantle flow around the high velocity slab  
308 beneath the Gibraltar Arc imaged by tomography and a lithospheric contribution acquired  
309 during the Western Mediterranean subduction in Eocene times. However, new results from  
310 both teleseismic and Pn tomographic studies do not seem to support the last point. Bezada et  
311 al. (2013) and Villaseñor et al. (2011), using new data from the TopoIberia and Picasso  
312 experiments, have produced new teleseismic 3D tomographic images that clearly refine the  
313 previous ones. A high velocity slab is identified beneath the Alboran Sea and the eastern  
314 Betics down to at least 600 km. Below 100 km, this slab is almost vertical and has an arcuate  
315 geometry following the arc from the eastern Betics to the Rif. Above this depth, the anomaly

316 can hardly be identified beneath the Betics, while it is clearly observed to the East of the Strait  
317 of Gibraltar, where it seems to be connected to the surface. This geometry supports the  
318 presence, already pointed out by Spakman and Wortel (2004), of slab tearing beneath the  
319 eastern Betics, which has also been proposed by Garcia-Castellanos and Villaseñor (2011),  
320 based on uplift rates in the Betics and the Rif. Pérouse et al. (2010) proposed a dynamic  
321 modeling of the western Mediterranean to account for GPS observations in which the slab is  
322 detached beneath the Betics but remains coupled beneath the Rif. The Pn tomography results  
323 presented by Díaz et al. (2013) show a large low velocity anomaly at the uppermost mantle  
324 beneath the eastern Betics which can be related to hot materials filling the zone where the slab  
325 is detached. Therefore, it seems now difficult to explain the anisotropy parameters observed  
326 along the arc as corresponding to a vertically coherent anisotropy acquired during the  
327 formation of the Gibraltar arc and preserved in the lithosphere, in particular if we note that  
328 eastern Betics is one of the zones with maximum observed delay times. It seems more  
329 plausible to explain the observations of Díaz et al. (2010), as well as the additional data  
330 presented by Miller et al. (2013), as the result of asthenospheric flow deflected around the fast  
331 velocity slab, located east of the Strait of Gibraltar (Figure 4b). The detachment of the slab  
332 beneath the Eastern Betics justifies the presence of the hot material at subcrustal levels, which  
333 can contribute to the strong anisotropic signature observed beneath this area (Figure 4c). Even  
334 if very different models have been proposed to explain the tectonic evolution of the Gibraltar  
335 Arc (Andrieux et al., 1971, Platt and Vissers, 1989, Faccenna et al., 2004, Gutscher et al,  
336 2002, Carminati et al., 2012, Vergés and Fernandez 2012), there is now an overall agreement  
337 to explain the Betic-Rif orogen as a consequence of the Ligurian-Tethys subduction and a  
338 west or northwest oriented slab roll-back. Different analog and numerical models have shown  
339 that roll-back can result in arcuate FPD variations (Faccenna and Capitanio, 2013), and this  
340 mechanism has been proposed to explain the FPD rotation along the Calabrian Arc  
341 (Baccheschi et al., 2011). Even if the anisotropic pattern retrieved in our case is similar,  
342 results from different fields, from structural geology to volcanism or geodesy strongly argue  
343 against an ongoing rollback process in the Gibraltar Arc (Platt et al., 2013). Alpert et al.  
344 (2013) presented a geodynamic flow model in which the observed anisotropy pattern could be  
345 explained without invoking this slab rollback. However, large slab density contrast and  
346 viscosity values are needed to induce the flow deflection around the slab and the observed  
347 FPD beneath the southernmost Spain or at the Alhucemas region (aprox 35°N, 3°W) are only  
348 partially reproduced. Therefore we interpret that the observed anisotropy pattern as depicting  
349 present-day mantle flow around a fixed Gibraltar slab. The scarce anisotropic measurements

350 obtained from the OBSs deployed in the western section of the Alboran Sea show a small,  
351 roughly E-W oriented FPD which do not seem to follow the general arcuate trend observed  
352 onland. However, further OBS deployments are needed to assess this point, as the available  
353 results are not robust enough to be conclusive.

354 Away from the Gibraltar Arc, the FPD observed beneath southern Iberia, shifting from NE-  
355 SW in the West to ENE-WSW in the eastern part, can also result from mantle flow deflected  
356 around the fast velocity slab. Note that stations located further North, discussed previously,  
357 show a clearly different E-W trend. Stations in the transitional area (37-38°N, west of 4°W)  
358 have a clear NE-SW mean FPD but show significant backazimuthal variability, interpreted as  
359 an image of complexity and depicting the limit of the area affected by flow around the slab.  
360 At northern Morocco, FPD evidences a rather symmetrical image, depicting a NW-SE  
361 oriented mantle flow beneath the Rif and the Gharb basin. The abrupt change in FPD in  
362 northern coast of Morocco at about 3°W (Alhuceimas region) has been interpreted as  
363 indicating the flow around the southward edge of the slab (Díaz et al., 2010). Note that the  
364 northern edge of the slab does not result in a similar change in FPD.

365

366 The new anisotropic measurements beneath SW Portugal show a quite different anisotropic  
367 pattern, with small amount of anisotropy and a large percentage of “nulls”. Under the classical  
368 hypothesis, “nulls” are only expected for those SKS waves with backazimuths coincident with  
369 the fast or slow directions of anisotropy, oriented orthogonally. The presence of nulls over a  
370 large backazimuthal range, mixed with evidences of anisotropy for other events, suggest that a  
371 more complex anisotropy pattern does exist beneath this area. It has been proposed by  
372 different authors (Long et al., 2010, Wagner et al., 2012), that the presence of a significant  
373 number of nulls can be explained by a poorly organized asthenospheric flow or, more  
374 probably, by the presence of a predominantly vertical flow. Models based on potential fields  
375 (Fullea et al., 2010, Jiménez-Munt et al., 2011) have evidenced a large variation, exceeding  
376 100 km, in lithospheric thickness between SW Portugal and the Gulf of Cadiz. While in  
377 southern Portugal the lithospheric thickness is estimated in 100-110 km, beneath the central  
378 part of the Gulf it can reach 200 km. Such variation may activate small-scale convective cells  
379 and thus vertical flow in the upper asthenosphere, resulting in small indications of anisotropy.  
380 The OBSs in the Gulf of Cadiz show a complex pattern, with the westernmost one displaying  
381 a North-South FPD, while the rest of the instruments have grossly EW oriented FPDs, similar  
382 to what is observed in the Alboran Sea. Few measurements are available and hence those  
383 results must be taken with caution; however, such anomalous variations can be related to the

384 presence of vertical flow beneath SW Portugal, which would result in a complex anisotropy  
385 pattern.

386

387 Stations in the Moroccan Meseta, the western High Atlas and the Anti-Atlas show similar  
388 results, with small values of  $\delta t$ , significant differences in the FPD derived from individual  
389 events and a large amount of nulls for a broad range of backazimuths. Lithospheric models  
390 presented by Fullea et al., 2010, show a thinned lithosphere beneath the Middle and High  
391 Atlas, with a difference of 50-75 km with respect to the Gulf of Cadiz. The presence of a  
392 vertical offset of the lithosphere-asthenosphere interface at the flanks of the High-Atlas has  
393 been recently documented by Miller and Becker (2013). Missenard et al., (2011) have  
394 independently proposed the presence of edge-driven convective cells beneath the Atlas to  
395 account for volcanologic observations. The significant step in lithospheric thickness could  
396 justify the presence of such small scale vertical convective cells, which in turn allow  
397 explaining the large observed number of nulls. Miller et al. (2013) reported relatively large  
398 delays beneath the axis of the northern part of the High Atlas and proposed that it may be  
399 related to plume material channeled along the sub-lithospheric corridor from the Canary  
400 Islands hotspot previously suggested by Duggen et al., (2009). The new stations analyzed in  
401 the central part of the High Atlas show mean  $\delta t$  values close to 1.0 s, similar to the values  
402 obtained in the Middle Atlas, but only a small amount of anisotropy is observed beneath the  
403 western High Atlas and in the Moroccan Meseta, with FPD showing a general ENE-WSW  
404 FPDs orientation,  $\delta t$  values clearly below 1.0s and a large number of nulls. This seems  
405 inconsistent with the hypothesis of a sub-lithospheric corridor, which should be present not  
406 only beneath the western High Atlas but all along its path from the Canary Islands. We prefer  
407 to interpret the anisotropic observations for the stations in the Anti-Atlas domain in terms of  
408 vertical flow in the mantle, associated to the very significant change in the elastic thickness  
409 beneath the northern rim of the WAC identified by Pérez-Gussinyé et al. (2009).

410

411

## 412 **5 Conclusions**

413

414 The knowledge of the anisotropic parameters beneath the Western Mediterranean region,  
415 from the Western African Craton to the Variscan core of Iberia is significantly improved by  
416 the new anisotropic measurements gathered at more than 100 new sites, including permanent

417 broad-band stations, the regularly spaced TopoIberia-Ibearth seismic network and additional  
418 temporary networks deployed over the area. Those new results provide an enlarged view of  
419 the regional geodynamic setting and allow a review of the previously proposed geodynamic  
420 models.

421

422 The anisotropic parameters here presented can be globally related to the LPO of mantle  
423 minerals generated by mantle flow at asthenospheric depths, even if different processes must  
424 be invoked to explain the observations (Figure 5). Beneath central Iberia, an area quite stable  
425 tectonically, the anisotropic parameters are rather uniform and cannot be related to the  
426 deformation inherited from the Variscan orogeny, the last large-scale tectonic event affecting  
427 the zone. The E-W oriented FPD seems compatible with the Conrad and Behn (2010) mantle  
428 flow model, which is computed from a combination of mantle flow fields driven by relative  
429 plate motions, mantle density heterogeneity and net lithosphere rotation. On the contrary,  
430 those FPD are not consistent with classical mantle flow models using NNR nor hotspot  
431 framed models to prescribe surface boundary conditions, as those used in Alpert et al. (2013).  
432 Further South, the data presented by Díaz et al. (2010), Miller et al. (2013) and Alpert et al.  
433 (2013) are discussed together taking into consideration recent results coming from teleseismic  
434 and Pn tomography, uplift rates or GPS measured relative displacements, which suggest that  
435 most of the observed anisotropy is probably due to mantle flow at different levels of the  
436 mantle. The arcuate variation of the FPDs following the Gibraltar Arc results from the mantle  
437 deflection around the fast velocity slab extending down to 600 km. Large delays are observed  
438 beneath the eastern Betics, in an area where tearing has been proposed and where Pn  
439 tomography shows the presence of hot materials, suggesting that uppermost mantle materials  
440 can contribute to the observed anisotropy. The small degree of anisotropy and the large  
441 number of observations without evidences of anisotropy beneath SW Iberia, the High Atlas  
442 and the northern rim of the West African Craton suggest the presence of vertical mantle flow  
443 associated to edge-driven convective cells triggered by large variations of the lithospheric  
444 thickness. It is important to note that many of the investigated stations show significant  
445 backazimuthal variations in the anisotropic parameters retrieved from single events. The  
446 analysis of those variations is beyond the objectives of this contribution, but previous work  
447 has shown that they can often be explained by the presence of multiple anisotropic layers,  
448 suggesting that lithospheric and asthenospheric contributions may coexist, at least beneath  
449 some regions.

450

451

452 **Acknowledgments**

453

454 We want to acknowledge all the field and processing Spanish and Moroccan teams of the  
455 TopoIberia-Iberarray experiment to make available this large dataset. We are also grateful to  
456 Christine Thomas and Ingo Grevemeyer to give us access to the data of their temporary  
457 experiments. CoMITAC is a multidisciplinary project funded by the European Research  
458 Council (ERC Grant 240473). The OBS deployment was part of ESF initiative TOPO-  
459 EUROPE/TOPO-MED and funded by the German Science Foundation (DFG grant  
460 GR1964/12-1). We want also to acknowledge the institutions responsible for the maintenance  
461 of the different permanent seismic networks contributing data to this study (Instituto  
462 Geográfico Nacional, Real Observatorio de la Armada, Instituto Andaluz de Geofísica, and  
463 Portuguese Seismic Network). This is a contribution of the Consolider-Ingenio 2010 project  
464 TOPO-IBERIA [CSD2006-00041]. Additional funding is provided by projects RIFSIS  
465 [CGL2009-09727], Siberia [CGL2006-01171] and Topomed [CGL2008-03474-E/BTE, ESF-  
466 Eurocores 07-TOPOEUROPE-FP006]. Most of the figures were produced using the Generic  
467 Mapping Tools (GMT) software (Wessel & Smith 1998).

468

469 **Figure Captions**

470

471 **Figure 1:** Topographic/bathymetric map of the investigated area. Blue dots show the location  
472 of TopoIberia stations with previously published anisotropic parameters. Red dots are for  
473 TopoIberia stations contributing to this work. Yellow dots account for permanent broad-band  
474 stations here analyzed. Black dots show the positions of temporary networks deployed as part  
475 of the Comitac project (High Atlas and Anti-Atlas) as well as the OBS deployed in the  
476 Alboran Sea and Gulf of Cadiz. Black diamonds show the PICASSO project stations,  
477 analyzed in terms of anisotropy by Miller et al. 2013.

478

479 **Figure 2:** Example of the splitting parameters obtained using the SplitLab software. a)  
480 Example of a good quality non-null measurement at station E054, located in eastern Iberia. b)  
481 Example of a fair quality event at station E053, also located in eastern Iberia. c) Example of  
482 “null” measurement at station M211, located in the Anti-Atlas domain.

483

484 **Figure 3:** Anisotropic parameters retrieved from our dataset overprinting a simplified tectonic  
485 map of the region. The results are presented in the projected location of the piercing point at a  
486 depth of 200 km. Bars are oriented along the FPD and their length is proportional to the  
487 measured  $\delta t$ . Red bars are for “good” quality measurements while orange bars stand for “fair”  
488 results. Null measurements are represented by thin black lines oriented along the  
489 backazimuth.

490

491 **Figure 4:** Sketch of the different processes invoked to explain the observed anisotropic  
492 parameters. Red lines account for the mean FPDs presented in this study and in Diaz et al  
493 2010. Blue lines show the FPDs calculated by Miller et al. 2013. Black lines are for the LPO  
494 direction derived from the Conrad and Behn (2010) global mantle flow model. a) Beneath  
495 central Iberia, the inferred FPD are in agreement with the proposed mantle flow, while they  
496 are not consistent with the APM in the no-net rotation and the fixed hotspot reference frames  
497 (Dark and light green arrows, respectively). b) The high velocity slab anomaly (blue  
498 shadowed area) imaged by seismic tomography beneath SW Iberia (Bezada et al. 2013) acts  
499 as a keel at upper mantle depths, deflecting the mantle flow around it (yellow arrows). c)  
500 Above 100 km the slab seems detached beneath the eastern Betics, allowing the presence of  
501 hot material at sublithospheric depths which can contribute to the total observed anisotropy.  
502 d) SW Iberia, the Morocco Meseta, western High Atlas and Anti-Atlas (brown contoured



503 areas) show small amount of anisotropy and large number of “nulls”. The color scale shows  
504 the percentage of nulls measurements for each station.

505

506 **Figure 5:** Cartoon depicting the main mantle flow pattern derived from the interpretation of  
507 our data. Green arrows account for the general direction of LPO deduced from the Conrad and  
508 Behn (2010) model. The blue body represents the fast velocity slab imaged by tomography,  
509 with dashed lines indicating 100 km depth intervals. Yellow arrows show the proposed mantle  
510 flow around the slab. Orange arrows represent the proposed small-scale vertical flow  
511 associated to changes in lithospheric thickness beneath SW Iberia and the western High Atlas  
512 and Anti-Atlas domains.

513

514

515

516

517

#### 518 **Supplemental Table Captions**

519

520 **Suppl. Figure 1:** Extended regional view of the available FPD data. Red lines account for the  
521 mean FPDs presented in this study and in Diaz et al 2010. Blue lines show the previously  
522 published FPDs as compiled in the Géosciences Montpellier's SplitLab Shear-wave splitting  
523 database (Wüstefeld et al., 2009). Black lines are for the LPO direction derived from the  
524 Conrad and Behn (2010) global mantle flow model

525

526 **Suppl. Table 1:** Geographical coordinates, mean fast polarization direction (FPD), standard  
527 deviation FPD, mean  $\delta t$ , standard deviation  $\delta t$ , number of “null”, number of total valid  
528 observations and time period analyzed for each of the investigated stations

529

530 **Suppl. Table 2:** Individual FPD and  $\delta t$  determinations for the stations not previously  
531 investigated. Event identifier, station code, station longitude, station latitude, backazimuth,  
532 quality factor (g for good, f for fair), FPD and  $\delta t$  derived from the rotation-correlation (RC)  
533 method, FPD and  $\delta t$  from the minimum energy method (ME) and preferred method.

534

535

536 **References:**

537

538 Alpert, L.A., Miller, M.S., Becker, T.W., and Allam, A. (2013). Structure beneath the  
539 Alboran from geodynamic flow models and seismic anisotropy, *J. Geophys. Res.*, 118, 4265-  
540 4277, doi:10.1002/jgrb.50309.

541

542 Anahnah, F., Galindo-Zaldivar, J., Chalouan, A. Pedrera, P. Ruano, J. Pous, J., Heise, W.,  
543 Ruiz-Constan, A., Benmakhlof, M., López-Garrido, A.C., Ahmamou, M.F., Sanz de  
544 Galdeano, C., Arzate, J., Ibarra, P., González-Castillo, L., Bouregba, N., Corbo, F., Asensio,  
545 E., (2011). Deep resistivity cross section of the intraplate Atlas Mountains (NW Africa): New  
546 evidence of anomalous mantle and related Quaternary volcanism, *Tectonics*, 30(TC5014),  
547 doi:10.1029/2010TC002859.

548

549 Andrieux, J., Fontboté, J.-M., Mattauer, M., 1971. Sur un modèle explicatif de l'Arc de  
550 Gibraltar. *Earth and Planetary Science Letters* 12, 191–198.

551

552 Baccheschi, P., Margheriti, L., Steckler, M.S. and Boschi, E. (2011). Anisotropy patterns in  
553 the subducting lithosphere and in the mantle wedge: A case study—The southern Italy  
554 subduction system. *J. Geophys. Res.*, 116, B08306, doi:10.1029/2010JB007961.

555

556 Barruol, G., Souriau, A., Vauchez, A., Díaz, J., Gallart, J., Tubia, J. and Cuevas, J. (1998).  
557 Lithospheric anisotropy beneath the Pyrenees from shear wave splitting *Journal of Geophys.*  
558 *Res.*, 103, 30039-30054

559

560 Barruol, G., Deschamps, A. and Coutant, O. (2004). Mapping upper mantle anisotropy  
561 beneath SE France by SKS splitting indicates Neogene asthenospheric flow induced by  
562 Apenninic slab roll-back and deflected by the deep Alpine roots. *Tectonophysics* 394, 125–  
563 138.

564

565 Becker, T. W. (2008), Azimuthal seismic anisotropy constrains net rotation of the lithosphere,  
566 *Geophys. Res. Lett.*, 35, L05303, doi:10.1029/2007GL032928.

567

568 Bezada, M.J., Humphreys, E.D., Toomey, D.R., Harnafi, M., Dávila, J.M., J. Gallart. J., 2013.  
569 Evidence for slab rollback in the westernmost Mediterranean from improved upper mantle  
570 imaging, *Earth Planet. Sci. Lett.*, 368, 51-60, doi:10.1016/j.epsl.2013.02.024  
571

572 Buforn, E., Bezzeghoud, M., Udías, A. and Pro, C. (2004). Seismic Sources on the Iberia-  
573 African Plate Boundary and their Tectonic Implications. *Pure appl. geophys.* 161, 623–646.  
574 Doi: 10.1007/s00024-003-2466-1  
575

576 Buontempo, L., G.H.R Bokelmann, G. Barruol and J. Morales, (2008). Seismic anisotropy  
577 beneath southern Iberia from SKS splitting. *Earth Planet. Int.*, 273, 237-250.  
578

579 Calvert, A., E. Sandvol, D. Seber, M. Barazangi, F. Vidal, G. Alguacil and N. Jabour (2000).  
580 Propagation of regional seismic phases [Lg and Sn] and Pn velocity structure along the  
581 Africa–Iberia plate boundary zone: tectonic implications. *Geophys. J. Int.* 142, 384–408.  
582

583 Carminati, E., Lustrino, M. and Doglioni, C (2012). Geodynamic evolution of the central and  
584 western Mediterranean: Tectonics vs. igneous petrology constraints. *Tectonophysics* 579  
585 (2012) 173–192  
586

587 Conrad, C. P., and M. D. Behn (2010), Constraints on lithosphere net rotation and  
588 asthenospheric viscosity from global mantle flow models and seismic anisotropy, *Geochem.*  
589 *Geophys. Geosyst.*, 11, Q05W05, doi:10.1029/2009GC002970.  
590

591 Dewey, J.F., Helman, M.L., Turco, E., Hutton, D.H.W. & Knott, S.D., (1989). Kinematics of  
592 the Western Mediterranean, in *Alpine Tectonics*, pp. 265–283, eds Coward, M.P., Dietrich, D.  
593 & Park, R.G., *Geol. Soc. Spec. Publ.*45, London.  
594

595 Díaz, J., A. Hirn, J. Gallart, J. and B. Abalos (1996). Upper mantle anisotropy in SW Iberia  
596 from long range seismic profiles and teleseismic shear-wave data. *Phys of the Earth and*  
597 *Planet Int.*, 95,153-166.  
598

599 Díaz, J., J. Gallart, A. Hirn, H. Paulssen et al., (1998). Anisotropy beneath the Iberian  
600 Peninsula: the contribution of the ILIHA NARS Broad-band Experiment. *Pure Appl.*  
601 *Geophys.* 151, 395–405.

602

603 Díaz, J., A. Villaseñor, J. Gallart, J. Morales, A. Pazos, D. Córdoba, J. Pulgar, J.L. García-  
604 Lobón, M. Harnafi and the TopoIberia Seismic Working (2009). The IBERARRAY  
605 broadband seismic network: a new tool to investigate the deep structure beneath Iberia.  
606 Orfeus Newsl. 8, 2.

607

608 Díaz, J., Gallart, J., Villaseñor, A., Mancilla, F., Pazos, A., Córdoba, D., Pulgar, J.A., Ibarra,  
609 P., Harnafi, M., (2010). Mantle dynamics beneath the Gibraltar Arc (western Mediterranean)  
610 from shear-wave splitting measurements on a dense seismic array, *Geophys. Res. Lett.*,  
611 37(L18304), doi:10.1029/2010GL044201.

612

613 Díaz, J., Gil, A and Gallart, J. (2013). Uppermost mantle seismic velocity and anisotropy in  
614 the Euro-Mediterranean region from Pn and Sn tomography. *Geophys. J. Int.*, 192, 310-325,  
615 doi: 0.1093/gji/ggs016

616

617 Duggen, S., Hoernle, K.A., Hauff, F., Klugel, A., Bouabdellah, M. and Thirlwall, M.F.,  
618 (2009). Flow of Canary mantle plume material through a subcontinental lithospheric corridor  
619 beneath Africa to the Mediterranean. *Geology*, 37, 283–286.

620

621 El moudnib, L.; Antonio Villaseñor; Mimoun Harnafi; Mohamed Majid Himmi; Josep Gallart  
622 (2012), Crust structure of northern Morocco and southern Iberian Peninsula from local  
623 earthquake tomography, Abstract T23F-2742 presented at 2012 Fall Meeting, AGU, San  
624 Francisco, Calif., 3-7 Dec.

625

626 Faccenna, C. and Capitanio, F.A. (2013). Seismic anisotropy around subduction zones:  
627 Insights from three-dimensional modeling of upper mantle deformation and SKS splitting  
628 calculations. *Geochem. Geophys. Geosyst.*, 14, doi:10.1029/2012GC004451.

629

630 Faccenna, C., C. Piromallo, A. Crespo-Blanc, L. Jolivet, F. Rossetti (2004). Lateral slab  
631 deformation and the origin of the Western Mediterranean arcs. *Tectonics* 23.  
632 doi:10.1029/2002TC001488.

633

634 Fichtner, A., Brian L.N. Kennett, Jeannot Trampert, Separating intrinsic and apparent  
635 anisotropy, *Physics of the Earth and Planetary Interiors*, 219, 2013, 11-20, doi:  
636 10.1016/j.pepi.2013.03.006.

637

638 Fullea, J., M. Fernández, J.C. Afonso, J. Vergés and H. Zeyen, (2010). The structure and  
639 evolution of the lithosphere–asthenosphere boundary beneath the Atlantic–Mediterranean  
640 Transition Region. *Lithos*, 120, 1-2, 74-95.

641

642 Gallart, J.; Gil; A., Díaz; J., Carbonell; R., Harnafi; M., Levander; A., Palomeras; I. and  
643 Córdoba, D. (2012). Variations of the crustal structure in the Rif cordillera, N-Morocco, from  
644 wide-angle seismic data. Abstract T32D-05 presented at 2012 Fall Meeting, AGU, San  
645 Francisco, Calif., 3-7 Dec.

646

647 Garcia-Castellanos, D., Villaseñor, A., (2011). Messinian salinity crisis regulated by  
648 competing tectonics and erosion at the Gibraltar Arc. *Nature* 480, 359–363.

649

650 Gibbons, W. and T. Morena, T. [eds] (2002). *The Geology of Spain*. Geological Society,  
651 London, 649 pp.

652

653 Gutscher, M.A., J. Malod, J.P. Rehault, I. Contrucci, F. Klingelhoefer, L. Mendes-Victor, L.  
654 and W. Spakman (2002). Evidence for active subduction beneath Gibraltar. *Geology* 30,  
655 1071–1074.

656

657 Kreemer, C. (2009), Absolute plate motions constrained by shear wave splitting orientations  
658 with implications for hot spot motions and mantle flow, *J. Geophys. Res.*, 114, B10405,  
659 doi:10.1029/2009JB006416.

660

661 Jiménez-Munt, I., M. Fernández, J. Vergés, D. Garcia-Castellanos, J. Fullea, M.  
662 Pérez-Gussinyé, and J. C. Afonso (2011), Decoupled crust-mantle accommodation of  
663 Africa-Eurasia convergence in the NW Moroccan margin, *J. Geophys. Res.*, 116, B08403,  
664 doi:10.1029/2010JB008105.

665

666 Long, M.D. and Becker, Th. W. (2010). Mantle dynamics and seismic anisotropy. *Earth and*  
667 *Planetary Science Letters* 297 (2010) 341–354. doi: 10.1016/j.epsl.2010.06.036

668

669 Long, M.D., Benoit, M.H., Chapman, M.C., King, S.D., (2010). Upper mantle anisotropy and  
670 transition zone thickness beneath southeastern North America and implications for mantle  
671 dynamics. *Geochem. Geophys. Geosyst.* 11, Q10012, <http://dx.doi.org/10.1029/2010GC003247>.

672

673 Mancilla, F., Daniel Stich, José Morales, Jordi Julià, Jordi Diaz, Antonio Pazos, Diego  
674 Córdoba, Javier A. Pulgar, Pedro Ibarra, Mimoun Harnafi and Francisco Gonzalez-Lodeiro  
675 (2012). Crustal thickness variations in northern Morocco. *J. Geoph. Res.*, 117, B02312,  
676 doi:10.1029/2011JB008608

677

678 Michard, A., O. Saddiqi, A. Chalouan, Lamotte. D. Frizon de, (2008). *Continental Evolution:  
679 The Geology of Morocco. Structure, Stratigraphy, and Tectonics of the Africa-Atlantic-  
680 Mediterranean Triple Junction.* Springer-Verlag, Berlin Heidelberg 116: 404 p.

681

682 Miller, M. S. and T. W. Becker, (2013). Reactivated lithospheric-scale discontinuities localize  
683 dynamic uplift of the Moroccan Atlas Mountains. *Geology*. G34959.1, doi:10.1130/G34959.1

684

685 Miller, M. S., A. Allam, T. W. Becker, J. F. DiLeo and Wookey, J. (2013), Constraints on the  
686 tectonic evolution of the westernmost Mediterranean and northwestern Africa from shear  
687 wave splitting analysis, *Earth and Planet. Sci. Lett.*. doi: 10.1016/j.epsl.2013.05.036

688

689 Missenard, Y. and Cadoux, A. (2011). Can Moroccan Atlas lithospheric thinning and  
690 volcanism be induced by Edge-Driven Convection?. *Terra Nova*, 00, 1-8, doi:  
691 10.1111/j.1365-3121.2011.01033.x

692

693 Nicolas, A., Christensen, N.I., (1987). Formation of anisotropy in upper mantle peridotites. A  
694 review. In: Fuchs, K., Froidevaux, C. (Eds.), *Composition, Structure and Dynamics of the  
695 Lithosphere–Asthenosphere System.* AGU, Washington, pp. 137–154.

696

697 Palomeras, I.; Sally Thurner; Alan Levander (2012). PICASSO: Shear velocities in the  
698 Western Mediterranean from Rayleigh Wave tomography. Abstract T23F-2744 presented at  
699 2012 Fall Meeting, AGU, San Francisco, Calif., 3-7 Dec.

700

701 Pérez-Gussinyé, M., M. Metois, M. Fernández, J. Vergés, J. Fullea, A.R. Lowry, (2009).  
702 Effective elastic thickness of Africa and its relationship to other proxies for lithospheric  
703 structure and surface tectonics, *Earth and Planetary Science Letters*, 287, 1–2, 152-167, doi:  
704 /10.1016/j.epsl.2009.08.004.  
705  
706 Pérouse, E., Vernant, Ph., Chéry, J. Reilinger, R. and McClusky, S. (2010). Active surface  
707 deformation and sub-lithospheric processes in the western Mediterranean constrained by  
708 numerical models. *Geology*, 38, 9, 823-826. Doi: 10.1130/G30963.1  
709  
710 Platt, J.P. and R.L.M. Vissers (1989). Extensional collapse of thickened continental  
711 lithosphere: An hypothesis for the Alboran Sea and Gibraltar arc, *Geology*, 17, 540-543.  
712 Savage, M.K. (1999). Seismic anisotropy and mantle deformation: what have we learned from  
713 shear wave splitting? *Rev. Geophys.* 37, 65–106.  
714  
715 Platt, J.P., Whitney M. Behr, W.M., Johanesen, K. and Williams, J.R. (2013). The Betic-Rif  
716 Arc and Its Orogenic Hinterland: A Review. *Annu. Rev. Earth Planet. Sci.* 2013. 41:14.1–  
717 14.45. Doi: 10.1146/annurev-earth-050212-123951  
718  
719 Ruiz-Constán, A., A. Pedrera, J. Galindo-Zaldívar, J. Pous, J. Arzate, F. J. Roldán-García, C.  
720 Marin-Lechado, and F. Anahnah (2012), Constraints on the frontal crustal structure of a  
721 continental collision from an integrated geophysical research: The central-western Betic  
722 Cordillera (SW Spain), *Geochem. Geophys. Geosyst.*, 13, Q08012,  
723 doi:10.1029/2012GC004153.  
724  
725 Savage, M.K., 1999. Seismic anisotropy and mantle deformation: what have we learned from  
726 shear wave splitting? *Rev. Geophys.* 37, 65–106.  
727  
728 Sallarès, V., A. Gailler, M.-A. Gutscher, D. Graindorge, R. Bartolomé, E. Gràcia, J. Díaz, J. J.  
729 Dañobeitia and N. Zitellini (2011). Seismic evidence for the presence of Jurassic oceanic crust  
730 in the central Gulf of Cadiz (SW Iberian margin) *Earth Planetary Science Letters*,  
731 doi:10.1016/j.epsl.2011.09.003  
732

733 Serrano, I., T.M. Hearn, J. Morales and F. Torcal (2005). Seismic anisotropy and velocity  
734 structure beneath the southern half of the Iberian Peninsula. *Phys. Earth and Planet. Int.*, 150,  
735 317-330.

736

737 Spakman, W. and M.J.R. Wortel, (2004). A tomographic view on western Mediterranean  
738 geodynamics. In: Ziegler, P. [Ed.], *The TRANSMED Atlas — The Mediterranean region*  
739 *from crust to mantle*. Springer, Berlin Heidelberg, pp. 31–52.

740

741 Thurner, S.; Imma Palomeras; Alan Levander (2012). Crustal and Lithospheric Structure of  
742 the Western Mediterranean: Pds Receiver Function Results from the PICASSO Experiment.  
743 Abstract T32D-06 presented at 2012 Fall Meeting, AGU, San Francisco, Calif., 3-7 Dec.

744

745 Tian, X., Zhang, J., Si, S., Wang, J., Chen, Y. and Zhang, Z. (2011). SKS splitting  
746 measurements with horizontal component misalignment. *Geophys. J. Int.*, 185, 1, 329-340.  
747 Doi: 10.1111/j.1365-246X.2011.04936.x

748

749 Verges, J. and Fernandez, M.,(2012). Tethys–Atlantic interaction along the Iberia–Africa  
750 plate boundary: The Betic–Rif orogenic system. *Tectonophysics*, 579, 144-172. Doi:  
751 10.1016/j.tecto.2012.08.032

752

753 Villaseñor, A., S. Chevrot, M. Harnafi, J. Gallart, and Topo-Iberia Seismic Working Group,  
754 Seismic structure beneath the Gibraltar Arc, Western Mediterranean region using broadband  
755 data from IberArray and permanent networks,(2011). *Geophysical Research Abstracts*, Vol.  
756 13, EGU2011-8420, EGU General Assembly 2011, Vienna, Austria.

757

758 Vinnik, L. P., R. Kind, G. L. Kosarev, and L. I. Makeyeva, (1989). Azimuthal anisotropy in  
759 the lithosphere from observations of long-period S-waves, *Geophys. J. Int.*, 99, 549–559

760

761 Wagner, L.S., Long, M. Johnston, M.D. and Benioit, M.H. (2012). Lithospheric and  
762 asthenospheric contributions to shear-wave splitting observations in the southeastern United  
763 States. *Earth Planet. Sci. Lett.*, 341-344, 128-138. doi: 10.1016/j.epsl.2012.06.020

764

765 Wessel, P. & Smith, W.H.F., 1998. New, improved version of the generic mapping tool  
766 released, *Eos, Trans. Am. geophys. Un.*, 47, 576.



767

768 Wüstefeld A., G. Bokelmann, Ch. Zaroli and G. Barruol (2006). SplitLab: A shear-wave  
769 splitting environment in Matlab, Computers & Geosciences, 34, 515-528.

770

771 Wüstefeld, A.; Bokelmann, G. H. R.; Barruol, G.; Montagner, J.-P. (2009) "Identifying global  
772 seismic anisotropy patterns by correlating shear-wave splitting and surface waves data" ,  
773 Phys. Earth Planet. Int, 176 (3-4), 198-212, doi:10.1016/j.pepi.2009.05.006 (database  
774 available online at <http://www.gm.univ-montp2.fr/splitting/DB/>)

## \*Highlights (for review)

Anisotropy beneath Iberia and N Morocco related to mantle flow in the asthenosphere.

FPDs consistent with global mantle flow models outside the Gibraltar Arc.

The fast velocity slab beneath the Gibraltar Arc deflects mantle flow around it.

Possible presence of edge-driven convective cells beneath the High Atlas and SW Portugal.

Figure 1  
[Click here to download Figure: Figs\\_rev2\\_1.pdf](#)

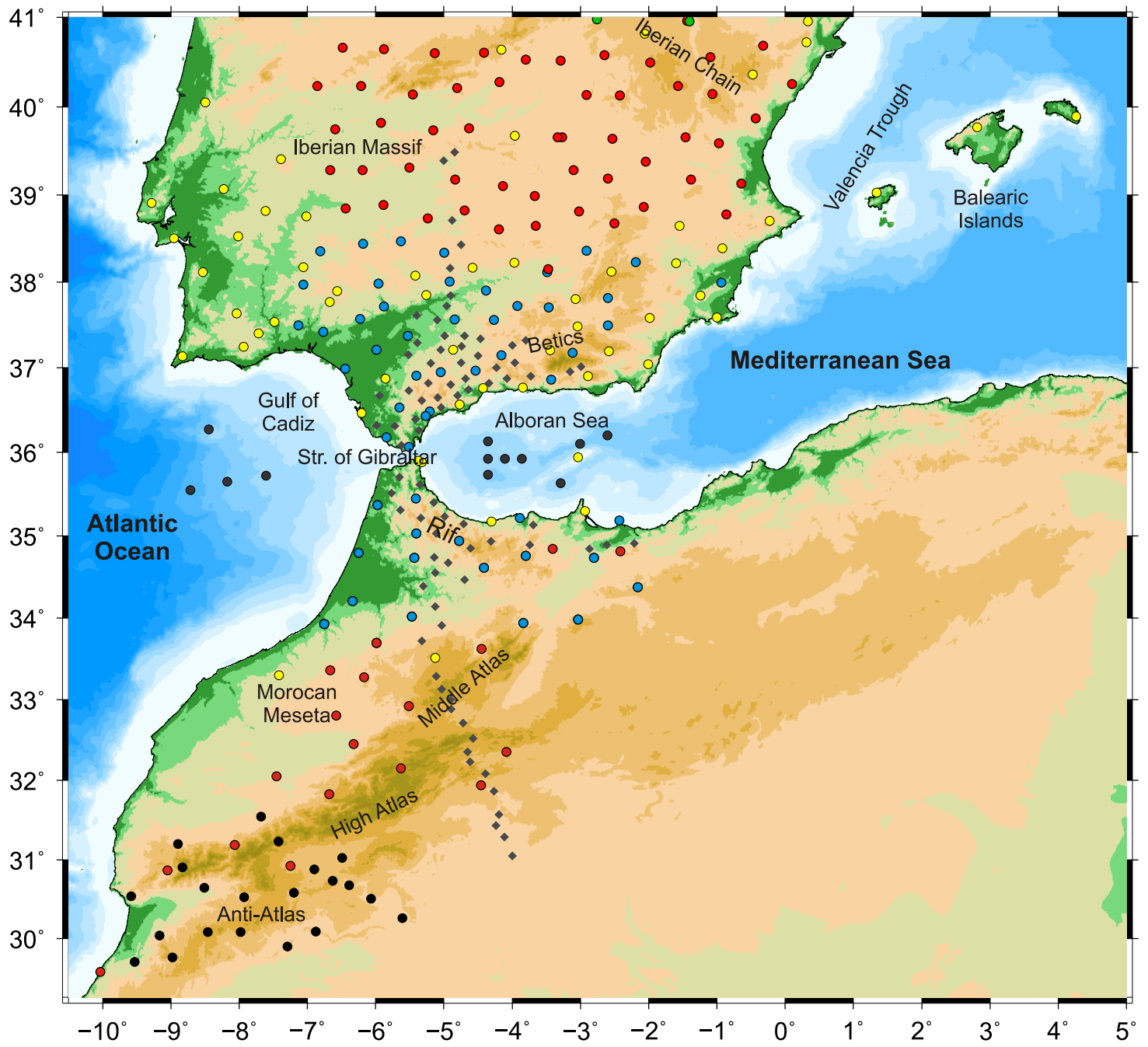
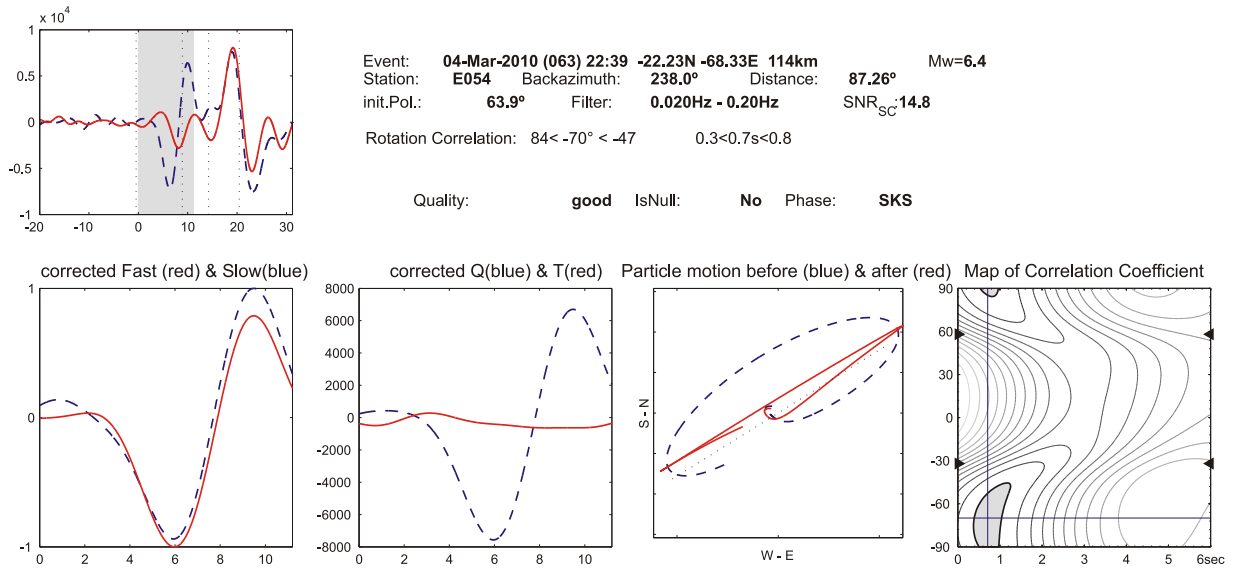


Figure 1

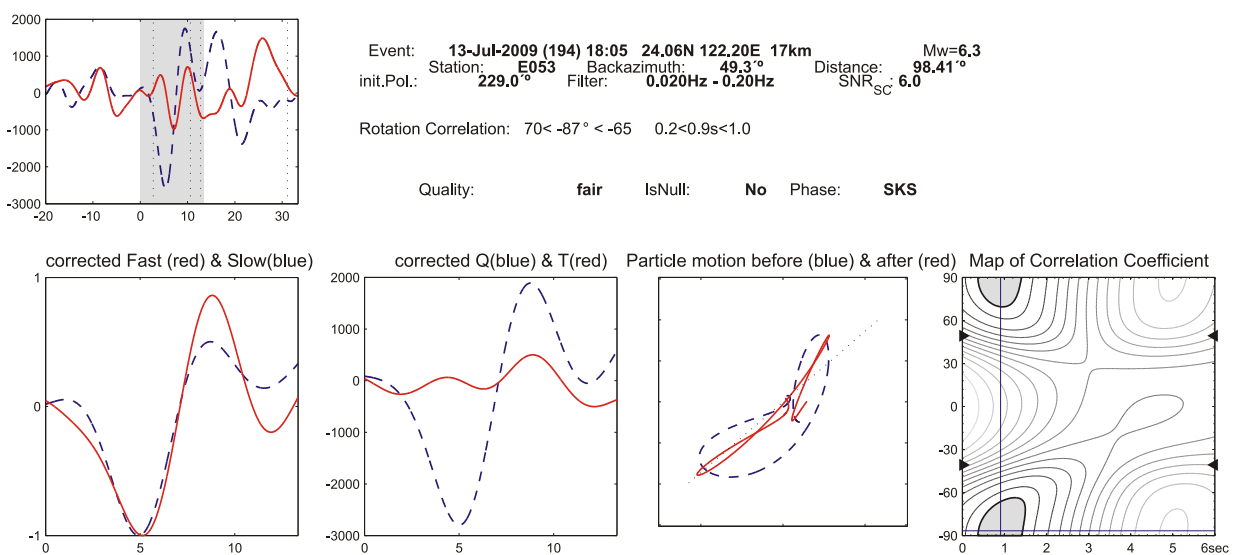
**Figure 2**

[Click here to download Figure: Figs\\_rev2\\_2.pdf](#)

**a)**



**b)**



**c)**

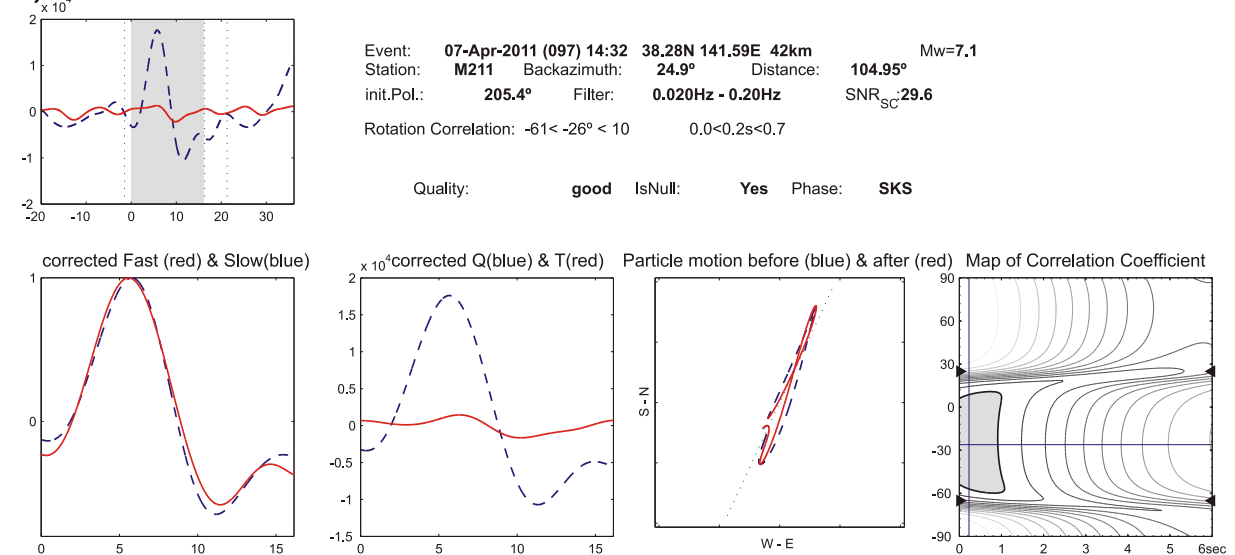


**Figure 2**

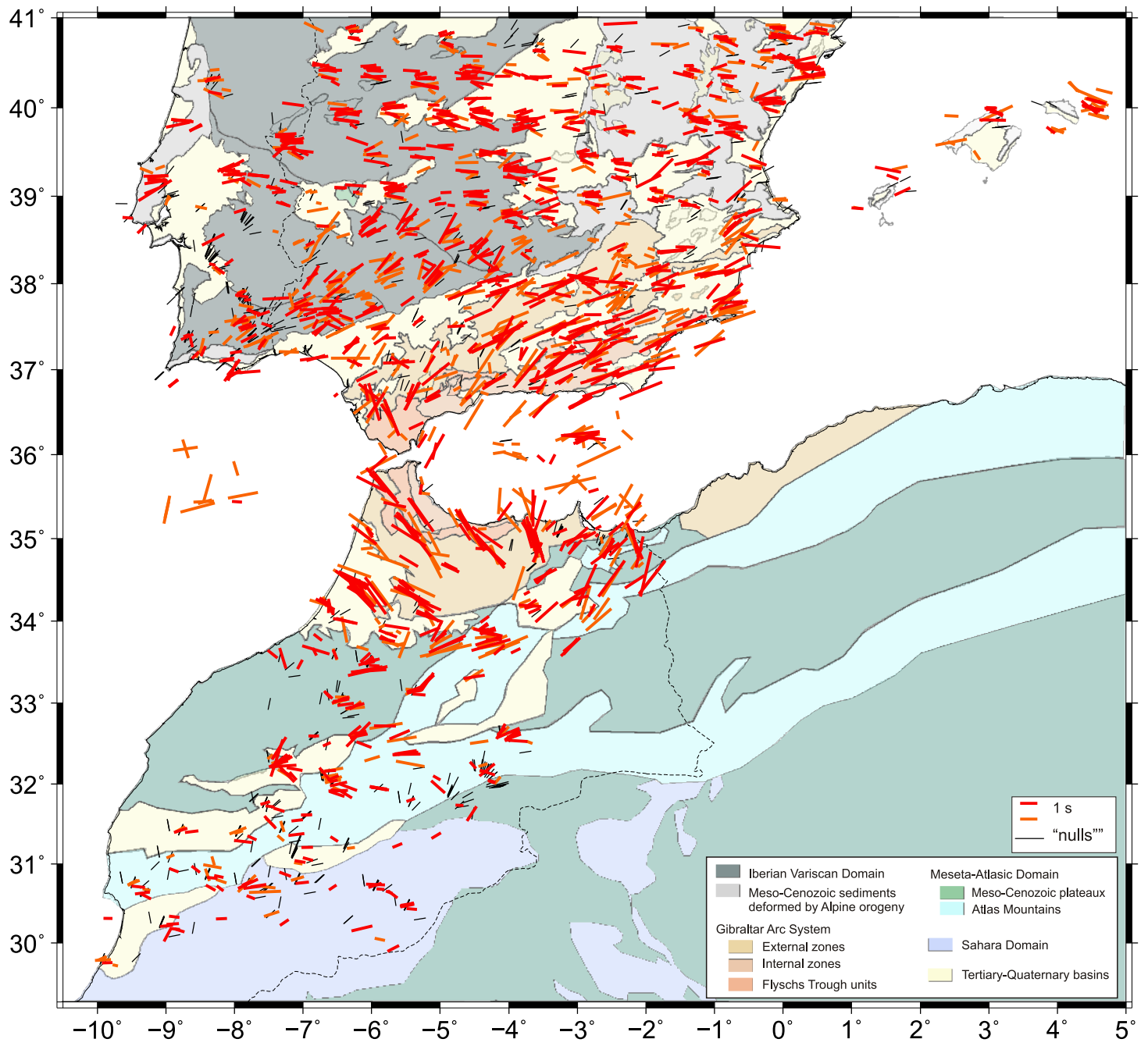


Figure 3

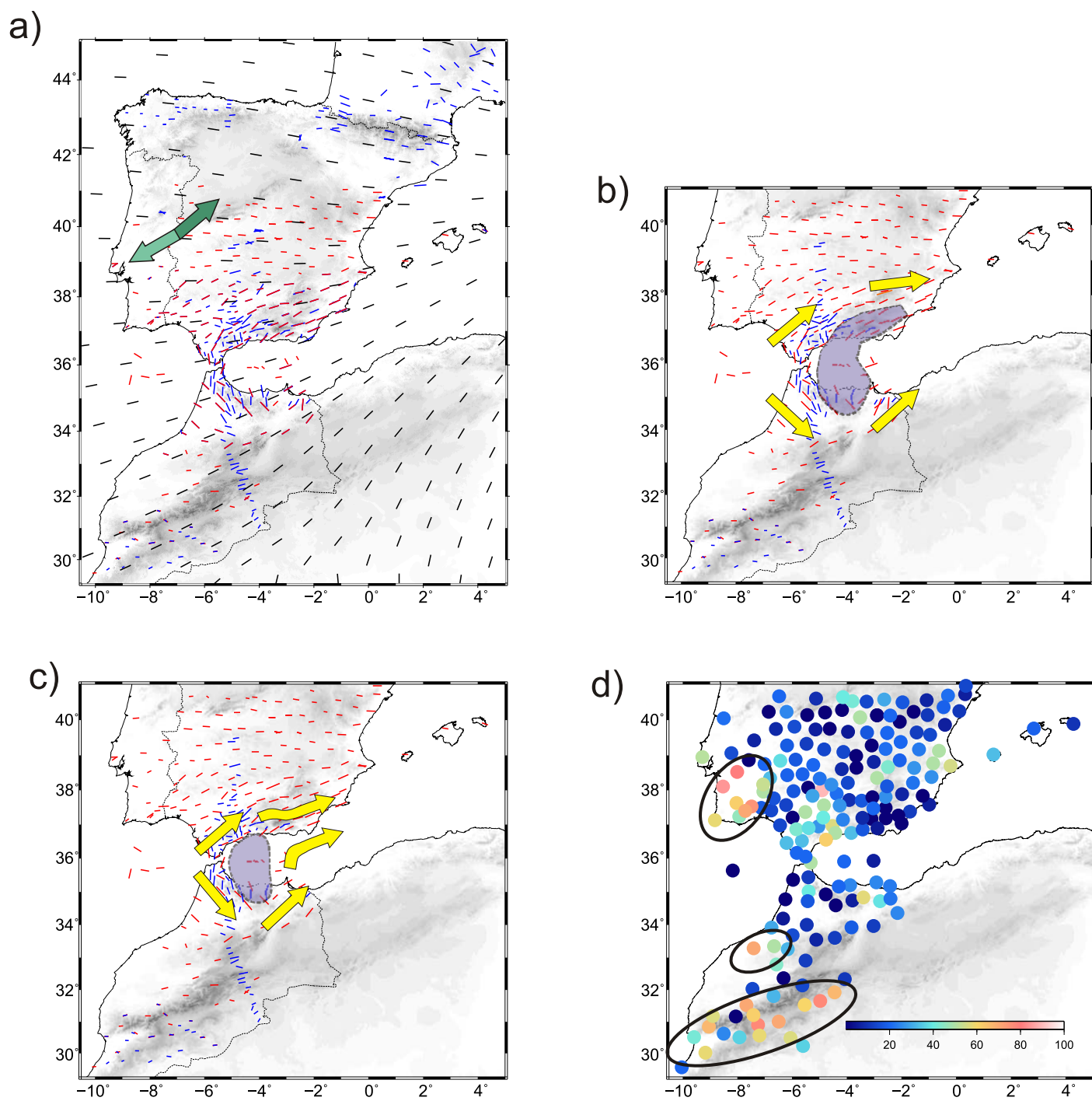


Figure 4

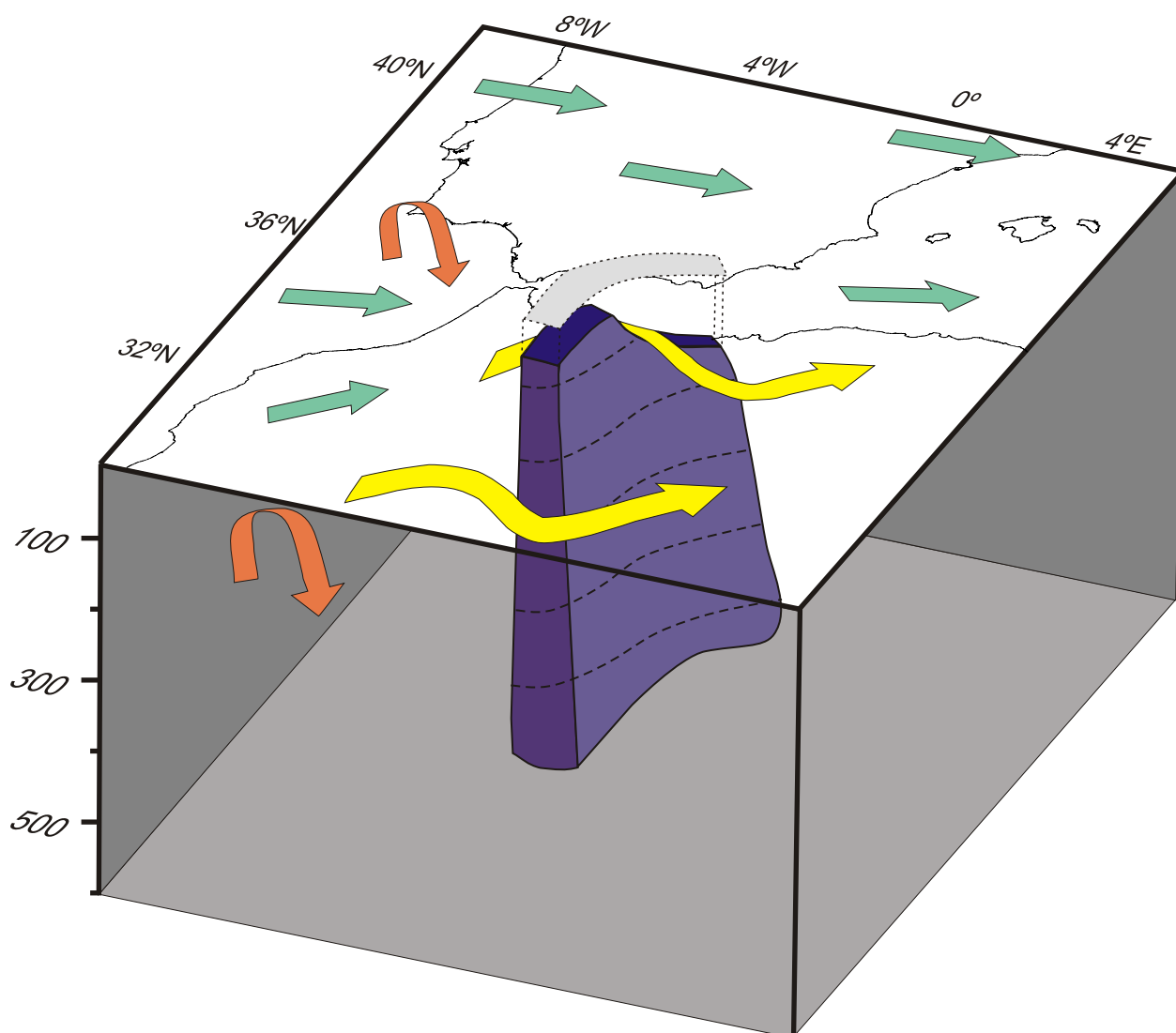


Figure 5